

## Research article

Dual role of citric acid: facilitate the bioconversion of CO<sub>2</sub> to CH<sub>4</sub> and enhance bioavailability of zero-valent iron

Despina Constantinou, Ioannis Vyrides \*

Cyprus University of Technology, Department of Chemical Engineering, Anexartisias 57 Str., 3603, Limassol, Cyprus

## ARTICLE INFO

**Keywords:**  
 Zero-valent iron  
 Citric acid  
 CO<sub>2</sub> bioconversion  
 Methanogenesis  
 Fe<sup>2+</sup>-citrate

## ABSTRACT

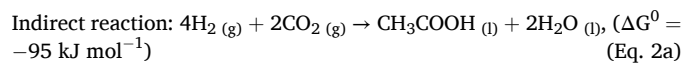
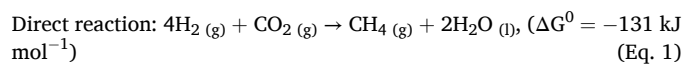
Studies on the bioconversion of CO<sub>2</sub> to CH<sub>4</sub> using Fe<sup>0</sup> have reported that a fraction of CO<sub>2</sub> is converted to FeCO<sub>3</sub>, forming a passivation layer on the Fe<sup>0</sup> surface, which reduces its reactivity and limits process efficiency. To mitigate FeCO<sub>3</sub> precipitation and enhance CO<sub>2</sub>-to-CH<sub>4</sub> conversion using Fe<sup>0</sup>, this study evaluates the role of citric acid (CA) as a ligand to Fe<sup>2+</sup>, which helps maintain iron in a soluble form and prevents its rapid conversion to insoluble iron carbonate (FeCO<sub>3</sub>). Batch experiments with 30 mM Fe<sup>0</sup>, anaerobic granular sludge (AGS), and NaHCO<sub>3</sub> with CA as a ligand showed that citrate biodegraded into acetic acid and CO<sub>2</sub> gas. To prevent citrate degradation and elucidate its effect on Fe<sup>0</sup>-mediated methanogenesis, 5% v/v of antibiotic antimycotic solution (100x) (10,000 units penicillin, 10 mg streptomycin and 25 µg amphotericin per ml) were introduced as a research tool, selectively inhibiting bacterial activity without affecting hydrogenotrophic methanogens. Methane production was notably enhanced only in the sample with NaHCO<sub>3</sub>, CA, antibiotics, and Fe<sup>0</sup>, reaching 38 ml by day 50, whereas the corresponding sample without Fe<sup>0</sup> produced only 22 ml, resulting in a net methane production of 16 ml. The results indicate that CA enhances methane production by maintaining iron solubility and inhibiting FeCO<sub>3</sub> precipitation, thereby facilitating continuous iron oxidation and sustained electron release, which supports the microbial reduction of CO<sub>2</sub> to CH<sub>4</sub>. While antibiotics provided a controlled environment to uncover these mechanisms, their use is not a viable long-term solution. Based on the findings of this study, future work may explore short-term CA exposure (<12 h) or alternative ligands to minimize biodegradation without relying on antibiotics.

## 1. Introduction

Global industrialization has driven economic growth and technological advancement but has also led to a 0.8 % increase in CO<sub>2</sub> emissions in 2022 (Energy Institute, 2023), intensifying global environmental issues. In response, engineers and researchers are exploring CO<sub>2</sub> capture and utilization (CCU) technologies to reduce carbon footprints. A promising technology is the conversion of CO<sub>2</sub> to CH<sub>4</sub>, which not only reduces CO<sub>2</sub> emissions but also generates a widely used energy carrier. The conversion can be achieved through either a catalytic (Dias and Perez-Lopez, 2021; Fang et al., 2023) or a biological process (Cheng et al., 2020; Jiang et al., 2022; Vyrides et al., 2018; Zabranska and Pokorna, 2018). However, biological CO<sub>2</sub> conversion operates at lower costs under ambient temperature and pressure conditions (Zabranska and Pokorna, 2018).

In the methanogenesis stage of anaerobic digestion (AD), the biological conversion of CO<sub>2</sub> to CH<sub>4</sub> occurs via two pathways (direct and

indirect) as follows (Jiang et al., 2022):



Direct pathway (Equation (1)) involves hydrogenotrophic methanogens, which metabolize H<sub>2</sub> and CO<sub>2</sub> to CH<sub>4</sub>, while indirect pathway (Equation (2a), (2b)) generates acetate as an intermediate product, which is subsequently metabolized by acetoclastic methanogens into biogas (Vyrides et al., 2018).

So far, numerous studies have demonstrated that zero-valent iron (ZVI) or (Fe<sup>0</sup>) serves various roles in AD and can effectively enhance methane production from waste-activated sludge (WAS) and improve

\* Corresponding author. Department of Chemical Engineering, Cyprus University of Technology, 57 Anexartisias Str., P.O. BOX 50329, 3603, Limassol, Cyprus.  
 E-mail address: [ioannis.vyrides@cut.ac.cy](mailto:ioannis.vyrides@cut.ac.cy) (I. Vyrides).

biogas production (Liu et al., 2015; Zhen et al., 2015). Fe<sup>0</sup> acts as a strong reducing agent ( $E^0 = -0.447$  V), and it contributes to maintaining oxidation-reduction potential (ORP) in a lower level ( $ORP < -0.3$  V), resulting in a more favorable environment for methanogens and other obligate anaerobic microbes (Baek et al., 2019; Tian and Yu, 2020). Notably, Fe<sup>0</sup> also contributes to the secretion of coenzyme F<sub>420</sub>, which is involved in the process of hydrogenotrophic methanogenesis (He et al., 2022).

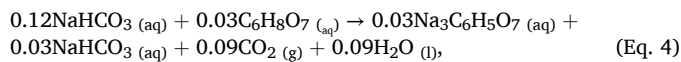
Fe<sup>0</sup> can be corroded under various environments, particularly in abiotic carbonate conditions, where it is oxidized, producing H<sub>2</sub> and forming FeCO<sub>3</sub> as a passivation layer on its outer surface, as shown on equation (3) (Constantinou et al., 2023). This process increases the availability of H<sub>2</sub>, which supports the growth of hydrogenotrophic microbes and subsequently enhances methane production (Tian and Yu, 2020).



Recently, there has been a growing interest in utilizing Fe<sup>0</sup> for the biological conversion of CO<sub>2</sub> into CH<sub>4</sub>. Vyrildes et al. (2018) studied the reduction of CO<sub>2</sub> gas into CH<sub>4</sub> using anaerobic granular sludge (AGS) and various concentrations of Fe<sup>0</sup>. After 18 days, 46 ml of CH<sub>4</sub> was produced at 75 g L<sup>-1</sup> Fe<sup>0</sup>, while 4 ml CH<sub>4</sub> was produced with no Fe<sup>0</sup> addition. Ma et al. (2018) evaluated the conversion of CO<sub>2</sub> to CH<sub>4</sub> in petroleum reservoir production waters at 55 °C for a duration of 16 days. The presence of Fe<sup>0</sup> in the samples resulted in methane production rates ranging from 61 to 79 μmol L<sup>-1</sup> d<sup>-1</sup>, while the corresponding controls without Fe<sup>0</sup> led to methane production rates of 0.6–0.12 μmol L<sup>-1</sup> d<sup>-1</sup>.

Although Fe<sup>0</sup> addition promotes CH<sub>4</sub> production, several studies have demonstrated the partial conversion of soluble CO<sub>2</sub> to FeCO<sub>3</sub> (siderite), forming a passivation layer on the Fe<sup>0</sup> surface. This layer reduces the Fe<sup>0</sup> corrosion, limits hydrogen generation, and consequently impedes CO<sub>2</sub>-to-CH<sub>4</sub> conversion (Dong et al., 2019; Ma et al., 2018; Vyrildes et al., 2018). Similar findings were reported by Menikea et al. (2020) and Zandt et al. (2019), indicating that FeCO<sub>3</sub> formation under both biotic and abiotic conditions acts as a protective barrier, decreasing Fe<sup>0</sup> reactivity. Dong et al. (2022) further highlighted that rapid corrosion of nano-ZVI accelerated the release of Fe<sup>2+</sup>/Fe<sup>3+</sup> ions. Consequently, these ions readily reacted with dissolved inorganic carbon, limiting CO<sub>2</sub> bioavailability and adversely affecting biomethanation efficiency. Ma et al. (2018) confirmed FeCO<sub>3</sub> formation via XPS analysis, suggesting chemical sequestration of CO<sub>2</sub> as siderite despite increased CH<sub>4</sub> production. Additionally, Zandt et al. (2019) highlighted the role of *Methanobacteriales* in mediating carbonate-rich layer formation on iron surfaces, contributing to corrosion control and long-term material stability.

Citric acid (CA) and ethylenediaminetetraacetic acid (EDTA) can be served as ligands to improve solubility of Fe and prevent the precipitation of Fe<sup>2+</sup> (Cai et al., 2019; Constantinou et al., 2023; Wang et al., 2023). Comparatively, CA offers the benefit of being environmentally friendly and cost-effective. Constantinou et al. (2023) demonstrated abiotic H<sub>2</sub> production with Fe<sup>0</sup> or scrap iron in the presence of trisodium citrate (generated via the reaction between NaHCO<sub>3</sub> and CA, according to equation (4)), forming stable, soluble Fe<sup>2+</sup>-citrate complexes. The resulting Fe<sup>2+</sup>-citrate complexes stabilize Fe<sup>0</sup> in solution, preventing its precipitation as FeCO<sub>3</sub> and thereby slowing down iron surface passivation to sustain H<sub>2</sub> generation over a longer period.



Wang et al. (2023) explored the enhancement of methane production from WAS by accelerating hydrogen corrosion of n-Fe<sup>0</sup> (nanoscale Fe<sup>0</sup>) using CA. The combined use of Fe<sup>0</sup> and CA increased methane yield by 63.8 % and hydrogen production by 2.42 times compared to using solo Fe<sup>0</sup>, demonstrating a substantial improvement in bioconversion

efficiency and suggesting a promising approach to boost biogas production through modified anaerobic digestion processes. However, Wang et al. (2023) did not consider that CA itself is biodegradable and may contribute directly to methane production. Gámez et al. (2009) demonstrated that in methanogenic anaerobic sludge, CA is primarily metabolized into acetic acid and CO<sub>2</sub>, with each mole of CA yielding 2 mol of acetate and 2 mol of CO<sub>2</sub>, both of which can further promote methanogenesis. Thus, part of the increased methane observed by Wang et al. (2023) may also be attributed to the biodegradation of CA, a factor that was not addressed. In the present study, this aspect was systematically examined.

This study aims to enhance the biological conversion of CO<sub>2</sub> to CH<sub>4</sub> using AGS in the presence of Fe<sup>0</sup> and CA as a chelating agent, with a particular focus on mitigating the formation of siderite, a known limitation in Fe<sup>0</sup> systems. While previous studies have demonstrated that CA improves iron solubility and boosts methane production, they have not accounted for the fact that CA is a biodegradable substrate and may also indirectly contribute to CH<sub>4</sub> generation through its degradation products. This dual role of CA — as both a ligand and a biodegradable substrate — has not been previously quantified or clearly separated. To address this research gap, the present study systematically investigates the biodegradation of CA and its impact on iron solubility, H<sub>2</sub> evolution, and methane production. Antibiotics were employed as a research tool to selectively inhibit bacterial activity and thus prevent CA degradation, enabling a clearer evaluation of its chelating effect. By separating the chemical and biological roles of CA, this study provides new insights into optimizing Fe<sup>0</sup>-assisted anaerobic digestion processes for improved CO<sub>2</sub>-to-CH<sub>4</sub> conversion efficiency.

## 2. Materials and methods

### 2.1. Inoculum source

Anaerobic granular sludge (13.37 % TS, 64.75 % VS of TS) was sourced from a full-scale internal circulation bioreactor treating dairy wastewater. Prior to use as an inoculum, the sludge was sieved and thoroughly washed with distilled water.

### 2.2. Experimental conditions

Batch laboratory experiments were performed in 165 ml anaerobic serum bottles with a working volume of 100 ml. All samples were capped and sealed with butyl septa and aluminum crimps, and subsequently, N<sub>2</sub> gas was introduced in the liquid phase for 1 min to ensure anaerobic conditions. All experiments were stirred in an incubator operating at 100 rpm and 34 ± 0.5 °C. Triplicate serum bottles were prepared for each experiment, except the control experiments, which were conducted in duplicates.

### 2.3. Experimental design

#### 2.3.1. Abiotic tests of hydrogen production by Fe<sup>0</sup> oxidation

Abiotic tests were conducted to assess the hydrogen production of three different solutions in the presence of 0.03 M Fe<sup>0</sup> (10 μm diameter) (Sigma Aldrich, CAS-No: 7439-89-6): (a) 0.12 M NaHCO<sub>3</sub> (Sigma Aldrich, code: S8875) (sample name: Bic-Fe), (b) 0.12 M NaHCO<sub>3</sub> and 0.03 M CA (Sigma Aldrich, code: C0759) (sample name: Bic-CA-Fe) and (c) 0.12 M NaHCO<sub>3</sub>, 0.03 M CA and 5 ml antibiotic solution (sample name: Bic-CA-Fe-ant). To maintain a 1:1 ratio between Fe<sup>0</sup> and citrate, the concentration of 0.03 M Fe<sup>0</sup> was selected based on the stoichiometry of the reaction between NaHCO<sub>3</sub> and CA, resulting in the formation of 0.03 M sodium citrate (Equation (4)).

#### 2.3.2. Evaluation of CA biodegradation prior to methanogenesis stage

Each serum bottle contained 5 g AGS, 0.12 M NaHCO<sub>3</sub> (as a source of CO<sub>2</sub>), 0.03 M CA, 0.36 M Fe<sup>0</sup> and 50 mM of 2-bromoethanesulfonate

(BES) (AGS-Bic-CA-Fe-BES) to eliminate the methanogenesis effect. Three background controls were prepared: (a) without  $\text{Fe}^0$ : 5 g AGS, 0.12 M  $\text{NaHCO}_3$ , 0.03 M CA and 50 mM BES (AGS-Bic-CA-BES) (b) without CA: 5 g AGS, 0.12 M  $\text{NaHCO}_3$ , 0.36 M  $\text{Fe}^0$  and 50 mM BES (AGS-Bic-Fe-BES) and (c) an abiotic system with 0.12 M  $\text{NaHCO}_3$  and 0.03 M CA (Bic-CA).

### 2.3.3. Assessment of different volumes of antibiotic antimycotic solution to inhibit CA biodegradation

Different volumes of antibiotic antimycotic solution (100x) (10,000 units penicillin, 10 mg streptomycin and 25  $\mu\text{g}$  amphotericin per ml – Sigma Aldrich, code: A5955): 1 %, 2.5 % and 5 % v/v were assessed as a strategy to inhibit bacteria and thus prevent the biodegradation of generated citrate. Each serum bottle contained 5 g AGS, 0.12 M  $\text{NaHCO}_3$ , 0.03 M CA and the tested amount of antibiotic solution.

### 2.3.4. Evaluation of CA as a complex agent for the bioconversion of $\text{CO}_2$ to $\text{CH}_4$ with $\text{Fe}^0$

This experiment evaluated the use of CA as a complex agent with  $\text{Fe}^0$  for the bioconversion of  $\text{CO}_2$  to  $\text{CH}_4$  in AGS. Therefore, (a) 5 g AGS, 5 ml antibiotic solution,  $\text{NaHCO}_3/\text{CA}$  (0.12 M/0.03 M) solution and 0.03 M  $\text{Fe}^0$  were introduced in the serum bottles (AGS-Bic-CA-ant-Fe). Two background controls were prepared as follows: (b) 5 g AGS,  $\text{NaHCO}_3/\text{CA}$  (0.12 M/0.03 M) solution and 0.03 M  $\text{Fe}^0$  (without antibiotic solution: AGS-Bic-CA-Fe) and (c) 5 g AGS,  $\text{NaHCO}_3$  (0.12 M) solution and 0.03 M  $\text{Fe}^0$  (without antibiotic solution and CA: AGS-Bic-Fe). Furthermore, the aforementioned solutions were conducted without  $\text{Fe}^0$  (consisted of AGS and the three different solutions only). No pH adjustments were implemented, as the aim was to observe the influence of CA in pH levels. Initial pH levels of solutions were (a)  $\text{NaHCO}_3/\text{CA}$  with antibiotics: 6.21, (b)  $\text{NaHCO}_3/\text{CA}$ : 6.26 and (c)  $\text{NaHCO}_3$ : 8.48.

## 2.4. Analytical methods

The gas phase constituents ( $\text{CH}_4$ ,  $\text{CO}_2$ ,  $\text{H}_2$ ,  $\text{N}_2$ ,  $\text{O}_2$ ) were identified and quantified over time by withdrawing 1 ml from the headspace and analyzing it using gas chromatography (Agilent Technologies 7820A GC system, Wilmington, DE) with the ShinCarbon ST packed column (Restek Corporation, Bellefonte, PA, USA) coupled to a thermal conductivity detector (GC-TCD) with argon as the carrier gas, as described by Constantinou et al. (2023).

The concentration of volatile fatty acids (VFAs) (formic, acetic, propionic, butyric and valeric acids) and citrate were analyzed over time using a High-Performance Liquid Chromatography (HPLC) system. The samples were filtered before analysis with 0.22  $\mu\text{m}$  acetate filters. The analysis used a Shimadzu LC-20AD liquid chromatography equipped with a Shimadzu SPD-20A UV/VIS detector, a Shimadzu SIL-20A HT autosampler, and a CTO-10AS VP column oven. A Rezex<sup>TM</sup> ROA-Organic Acid H<sup>+</sup> (8 %) column (Phenomenex, LC column 150  $\times$  7.8 mm) thermostated at 55 °C was used for chromatographic separation and elution was made isocratically with 5 mM  $\text{H}_2\text{SO}_4$  at a flow rate 0.7 ml min<sup>-1</sup> and an injection volume at 1  $\mu\text{L}$ .

To detect  $\text{Fe}^{2+}$  ions over time, a HACH UV/VIS scanning spectrophotometer (JENWAY 7315, Staffordshire, UK) on the wavelength of 562 nm was used, based on Stookey (1970) assay. To determine  $\text{Fe}^{3+}$  concentration,  $\text{Fe}^{3+}$  was reduced to  $\text{Fe}^{2+}$  using 20 g L<sup>-1</sup> ascorbic acid and the final  $\text{Fe}^{2+}$  was assayed with ferrozine reagent. Then, the concentration of  $\text{Fe}^{3+}$  was calculated as the difference between initial and final  $\text{Fe}^{2+}$  concentrations.

### 2.5. Microbial community analysis

At the end of batch experiments, an appropriate amount of sample (0.3–0.5 g) was withdrawn from each anaerobic serum bottle and the DNA extraction was performed using the NucleoSpin<sup>®</sup> Soil kit (MACHEREY-NAGEL, Germany), following the manufacturer's protocol

(MACHEREY-NAGEL. NucleoSpin<sup>®</sup> Soil kit – User Manual Rev. 05, Takara Bio, 2021). The samples were sent to Novogene (Cambridge, UK) for analysis. The V3–V4 region of bacterial and archaeal genes was amplified using primers 341F (5'-CCTACGGGRSGCAGCAG-3') and 806R (5'-GGACTACCAGGGTATCTAA-3'). PCR reactions included 30  $\mu\text{l}$  of master mix, 0.2  $\mu\text{M}$  primers, and ~10 ng of DNA. Amplification was carried out at 98 °C for 1 min, followed by 30 cycles of 10 s at 98 °C, 30 s at 50 °C, and 60 s at 72 °C, with a final elongation at 72 °C for 5 min. Purified PCR products were used for library preparation and sequenced on an Ion S5<sup>TM</sup> XL platform (Thermo Fisher, USA). Quality control was conducted with Cutadapt (v1.9.1), and sequences were clustered into operational taxonomic units (OTUs) at 97 % similarity using Uparse software. Taxonomic classification was performed with the SSURNA database at an 80 % confidence threshold.

## 3. Results and discussion

### 3.1. Abiotic tests for hydrogen production

Hydrogen production measurements were carried out for 50 days at regular intervals of approximately 2–4 days (Fig. 1), to assess the impact of  $\text{Fe}^0$  on  $\text{H}_2$  generation in three different solutions in the absence of AGS. Overall, abiotic tests showed that hydrogen was produced in all three systems (Bic-Fe, Bic-CA-Fe, and Bic-CA-Fe-ant). The Bic-CA-Fe sample exhibited the highest total hydrogen production, reaching 39.5 ml by day 50, and also demonstrated the most rapid  $\text{H}_2$  generation rate during the first 10 days. The Bic-CA-Fe-ant sample showed the second-highest hydrogen production rate during the early phase (first 10 days). In contrast, the Bic-Fe sample, which lacked citric acid, exhibited the slowest hydrogen production rate among the three during the first 10 days (Fig. 1).

Total soluble iron measurements indicated that  $\text{Fe}^{2+}$  was negligible in the Bic-Fe sample due to its precipitation as  $\text{FeCO}_3$  (Fig. 2a), as shown in Equation (3). In contrast, samples Bic-CA-Fe and Bic-CA-Fe-ant exhibited total soluble iron concentrations of 28.6 and 15.3 mM, (Fig. 2d), on day 50, respectively, with 79.4 % and 73.7 % of the total iron corresponding to  $\text{Fe}^{2+}$  species (Fig. 2b and c).

It is well established that acidic conditions promote the oxidation of metals (Khemkha et al., 2024). Therefore, the presence of CA seems to favor the oxidation rate of iron and consequently increase hydrogen production, since the resulting solution (tri-sodium citrate – based on Equation (4)) is more acidic than the  $\text{NaHCO}_3$  solution, with pH values of 6.2 and 8.5, respectively. Final pH value for the samples Bic-Fe, Bic-CA-Fe and Bic-CA-Fe-ant was 9.3, 8.5 and 7.7, respectively. Notably, citrate measurements were conducted for the abiotic samples, revealing that the concentration of citrate remained stable throughout the experiment. This indicates that citrate does not convert into a byproduct during the abiotic reaction with iron.

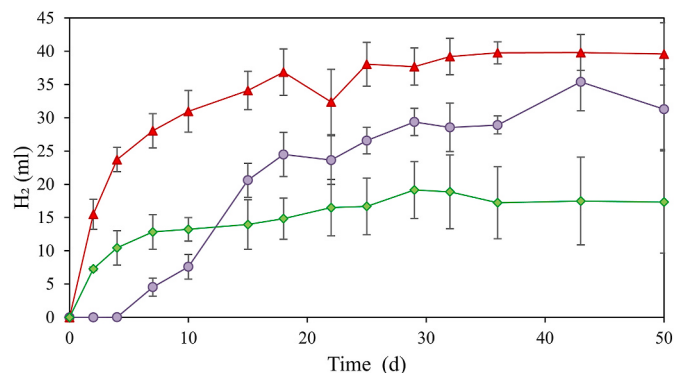
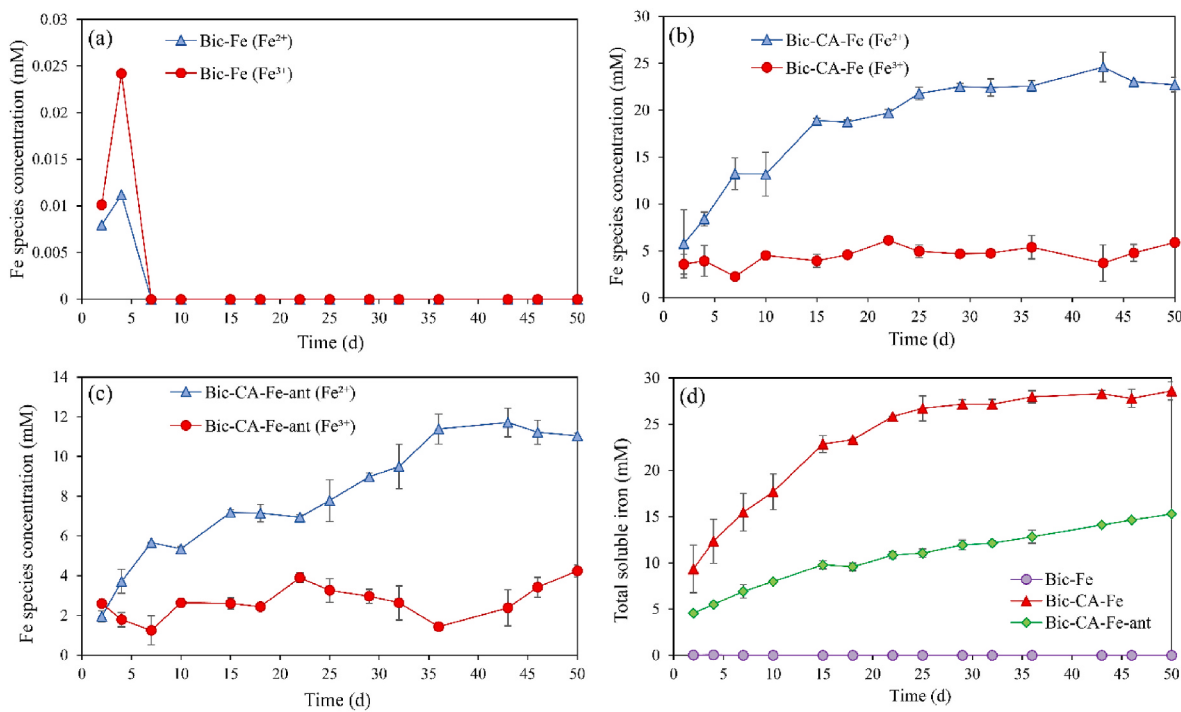


Fig. 1. Hydrogen (ml) production over time in the abiotic samples Bic-Fe (—●—), Bic-CA-Fe (—▲—) and Bic-CA-Fe-ant (—◆—).



**Fig. 2.** Concentration (mM) of iron species ( $\text{Fe}^{2+}$ ,  $\text{Fe}^{3+}$ ) in (a) Bic-Fe, (b) Bic-CA-Fe, (c) Bic-CA-Fe-ant and (d) total soluble iron (mM) concentration. Initial concentration of iron used was 30 mM.

Abiotic tests revealed that antibiotics significantly hinder iron activity, decreasing its solubility and reducing overall  $\text{H}_2$  production by at least 50 %. The lower cumulative hydrogen production observed in the Bic-CA-Fe-ant system may be attributed to surface passivation effects, where antibiotics likely interacted with the  $\text{Fe}^0$  surface, limiting its reactivity and slowing the overall corrosion process after the first 10 days. Nevertheless, the inclusion of antibiotics offers valuable insights into the system's behavior.

### 3.2. Citrate degradation prior to methanogenesis stage

To assess the degradation of citrate and the distribution of citrate carbon on the different intermediate products of AD, the methanogenesis was inhibited with BES. The degradation rate of citrate, as shown in Fig. 3, was slightly higher in the presence of  $\text{Fe}^0$  (Fig. 3b) compared to the sample without  $\text{Fe}^0$  (Fig. 3a). In both cases, citrate degradation in the presence of AGS primarily yielded acetic acid as the final liquid metabolite. Particularly, the acetic acid concentration in the presence of  $\text{Fe}^0$  was 85 mM, which is higher than the concentration without  $\text{Fe}^0$  (58.5 mM). This difference is attributed to the activity of homoacetogens, which consume  $\text{CO}_2$  and  $\text{H}_2$  produced in the presence of  $\text{Fe}^0$ , leading to an increase in acetic acid production.

Among other VFAs, formic acid in the presence of  $\text{Fe}^0$  peaked at 11.7 mM on day 3 before decreasing to zero by day 7. A similar trend was observed in the system without  $\text{Fe}^0$ , where on day 5 formic acid reached 5 mM and then gradually decreased (Fig. 3a and b). Propionic acid was detected at low concentrations (3.4 mM) in both samples (Fig. 3a and b). Similar results were obtained by Gámez et al. (2009), where in methanogenic sludge, the predominant metabolite of anaerobic degradation of citrate was acetic acid. In order to degrade CA in the absence of oxygen, bacteria have developed a pathway, which is initiated by citrate lyase that converts citrate into oxaloacetate and acetate. Following that, oxaloacetate is converted into pyruvate and  $\text{CO}_2$  by oxaloacetate decarboxylase (Gámez et al., 2009; Quintans et al., 2008).

Fig. 4a demonstrates that  $\text{CO}_2$  gas was produced abiotically in the Bic-CA (4:1) sample as equation (4) indicates.  $\text{CO}_2$  production reached

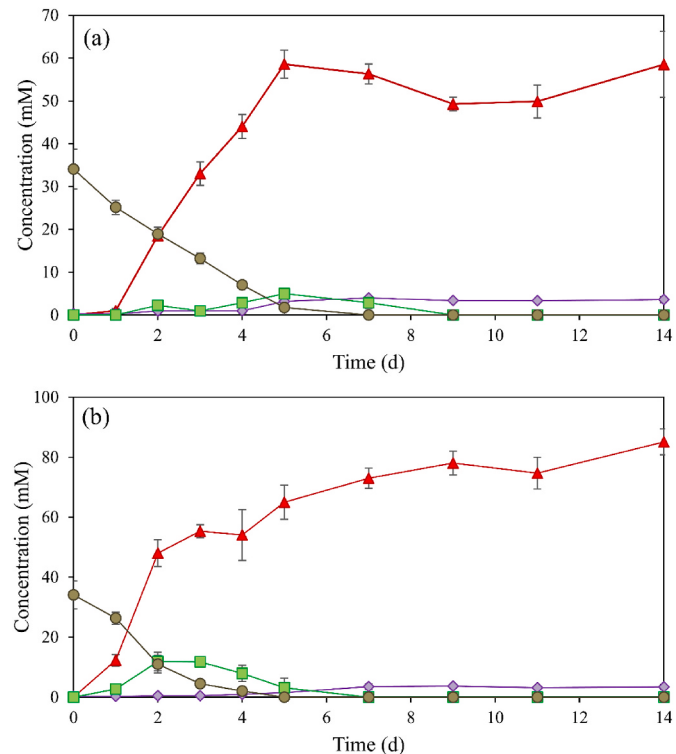


**Fig. 3.** Citrate degradation and VFAs production over time in the presence of AGS and  $\text{NaHCO}_3/\text{CA}$  (4:1) with 50 mM BES: (a) no  $\text{Fe}^0$  (AGS-Bic-CA-BES) and (b) 20  $\text{g L}^{-1}$  (0.36 M)  $\text{Fe}^0$  (AGS-Bic-CA-Fe-BES). Acetic acid (red triangle), propionic acid (purple diamond), formic acid (green square), and citrate (brown circle).

30 ml within 5 days and remained stable for the subsequent 14 days. Notably, the production rate was rapid, resulting in the generation of 23 ml of  $\text{CO}_2$  on day 1 (Bic-CA sample). A similar trend is observed in the

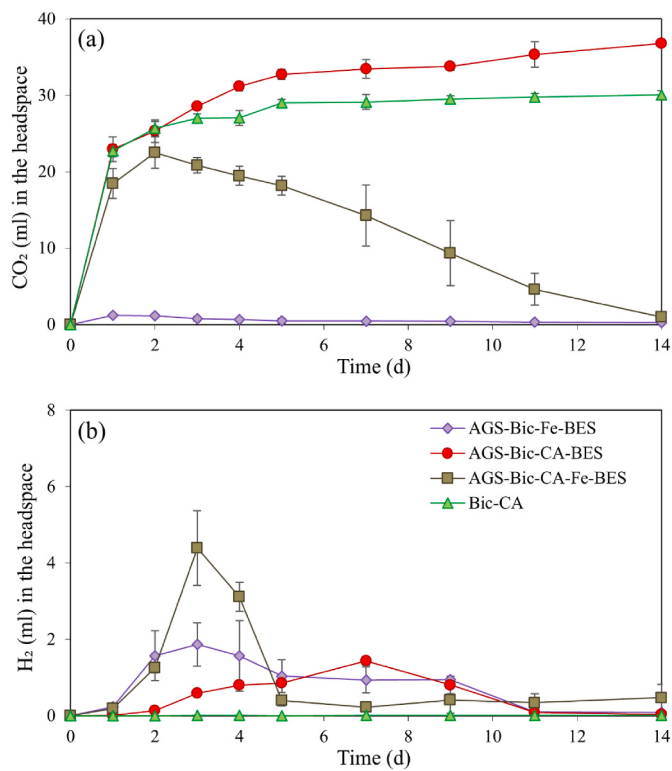


Fig. 4. (a) CO<sub>2</sub> (ml) and (b) H<sub>2</sub> (ml) in the headspace over time.

sample AGS-Bic-CA-BES, where the concentration of CO<sub>2</sub> remained stable (36 ml) over time. The observed difference of 6 ml between the two samples is likely due to the biodegradation of citrate to CO<sub>2</sub> in the presence of AGS. The sample containing Fe<sup>0</sup> and CA (AGS-Bic-CA-Fe-BES) produced the highest amounts of CO<sub>2</sub> and H<sub>2</sub> on day 2 (22.5 ml CO<sub>2</sub>) and day 3 (4.3 ml H<sub>2</sub>), respectively, with both gases gradually decreasing over time (Fig. 4a and b). This observation supports the notion that homoacetogens consume CO<sub>2</sub> along with H<sub>2</sub> to produce acetic acid through the homoacetogenesis pathway. In addition to the biological consumption, the reduction in CO<sub>2</sub> levels in the AGS-Bic-CA-Fe-BES sample may be attributed to its absorption into the liquid phase, as the pH increased from 6.20 to 8.92. The pH increase is a consequence of Fe<sup>0</sup> oxidation (Equation (3)), during which protons are consumed as H<sub>2</sub> is generated, thereby increasing alkalinity, and promoting the precipitation of CO<sub>2</sub> on the iron surface. Although CO<sub>2</sub> absorption typically lowers pH, the presence of Fe<sup>0</sup> results in a net pH increase. In contrast, in the AGS-Bic-Fe-BES sample, CO<sub>2</sub> gas generation is negligible (Fig. 4a), since the final pH was 9.4, resulting in CO<sub>2</sub> remaining predominantly in its soluble form.

In the system of AGS-Bic-Fe-BES without CA, the concentration of soluble iron remained negligible over the incubation time. In contrast, in the AGS-Bic-CA-Fe-BES system, concentrations of ferrous and ferric ions peaked at 2.6 mM and 7.2 mM, respectively, on day 3, before gradually decreasing due to precipitation (Supplementary Fig. 1). The initial high concentrations of soluble iron observed over the first four days were attributed to the formation of iron-citrate complexes. After day 4, the biodegradation of citrate by anaerobic microorganisms (as indicated in Fig. 3) led to the dissociation of these complexes, resulting in the subsequent precipitation of iron.

Wang et al. (2023) reported that the concentration of ferrous ions was 2.32 times higher in the presence of CA in WAS than that in the absence of CA. However, the amount of Fe<sup>2+</sup> measured (4.35 mg L<sup>-1</sup>) was negligible compared to the initially introduced quantity of n-Fe<sup>0</sup> (nano-Fe<sup>0</sup>) (1.68 g L<sup>-1</sup>). Based on the findings of this study, it is crucial to evaluate Fe<sup>0</sup> solubility through continuous monitoring over time, as

chelator biodegradation can significantly influence Fe<sup>0</sup> bioavailability. Relying on single or endpoint measurements may not capture the full dynamics of iron solubility and corrosion process.

### 3.3. Efficacy of antibiotics

Based on the results presented in Section 3.2., it was determined that citric acid facilitates the release of CO<sub>2</sub> when added with NaHCO<sub>3</sub> and further enhance H<sub>2</sub> production through Fe<sup>0</sup> corrosion. Additionally, the biodegradation of CA results in the generation of acetic acid, which could explain the enhanced performance observed in anaerobic digestion processes, as reported in several studies (Meng et al., 2024; Wang et al., 2023); a phenomenon that was overlooked in those studies. Therefore, to address the impact of CA biodegradation on the performance of Fe<sup>0</sup> systems, appropriate controls must be implemented. In this experiment, the use of antibiotics was tested as a research tool to inhibit CA biodegradation, thereby preserving its beneficial effects in enhancing Fe<sup>0</sup> performance and bioavailability. The approach of selectively inhibiting bacteria using antibiotics—without severely affecting methanogens—has also been adopted in other studies (Gao et al., 2024; Palacios et al., 2021; Vyrides et al., 2018; Xu et al., 2017) either to investigate specific microbial processes or to enhance methanogenic activity. Furthermore, the use of antibiotics to suppress bacterial populations is a well-established microbiological technique for facilitating the selective enrichment and isolation of methanogenic archaea from complex microbial communities (Kumar et al., 2012; Zhe et al., 2025).

Meng et al. (2024) reported that the hydrogenotrophic methanogens demonstrate a higher resilience to stress induced by high concentrations and complex compositions of antibiotics compare to bacteria. Based on this, the hypothesis is that hydrogenotrophic methanogens, which utilize H<sub>2</sub> and CO<sub>2</sub>, will remain unaffected by the antibiotics, whereas the bacteria responsible for the biodegradation of CA will be inhibited. As a result, it is expected that the overall system performance will be high.

Penicillin is a group of β-lactam antibiotics. β-lactam inhibitors can inhibit the synthesis of cell wall murein (peptidoglycan) by targeting penicillin-binding protein (Xiao et al., 2021), consequently rendering cells vulnerable to osmotic pressure and autolysis (Feng et al., 2023). A study by Lins et al. (2015) found no significant VFA accumulation and less than 10 % inhibition of CH<sub>4</sub> production, likely due to the distinct cell wall structure of methanogenic archaea, which makes them less susceptible to antibiotics than bacteria. Additionally, Viswanath and Nand (1989) showed that penicillin selectively inhibited acidogenic bacteria without affecting methanogens, due to their resistant cell wall structure, leading to reduced VFA accumulation and improved methane production. Therefore, penicillin antibiotics were employed to selectively inhibit bacterial activity while preserving methanogens, in order to prevent citrate degradation and enable a more precise examination of citric acid's role in Fe<sup>0</sup>-mediated CO<sub>2</sub>-to-CH<sub>4</sub> conversion.

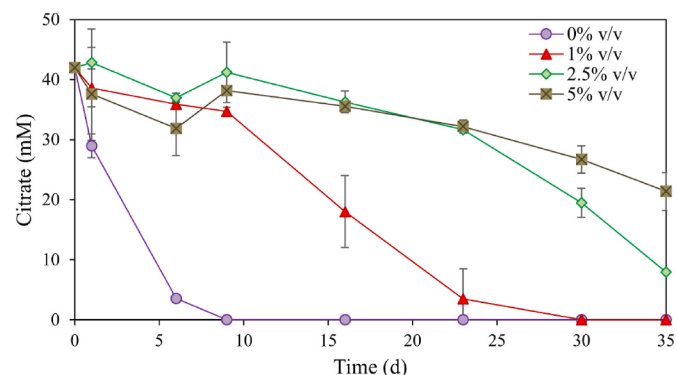


Fig. 5. Citrate degradation over time in the presence of AGS and NaHCO<sub>3</sub>/CA (4:1) solution under different concentrations of antibiotics.

Antibiotic concentrations 1 %, 2.5 % and 5 % v/v were tested in the presence of  $\text{NaHCO}_3/\text{CA}$  (4:1) and AGS. As Fig. 5 shows, the utilization of 1 % v/v antibiotics proved insufficient to effectively limit bacteria growth, since citrate was fully biodegraded within 30 days. The addition of 5 % v/v antibiotics was the most effective among the tested concentrations (Fig. 5) in significantly delaying citrate degradation for over 35 days. Although partial citrate degradation still occurred at 5 % v/v, higher antibiotic doses were not pursued. Beyond 5 % v/v, excessive chemical loading could lower pH, alter trace metal solubility, and reduce hydrogen generation (Fig. 1), compromising system stability without clear additional benefit. Moreover, the microbial response to higher streptomycin levels remains insufficiently defined, particularly regarding the resilience of methanogenic archaea under such stress. The 5 % v/v dosage corresponded to  $\sim 500 \text{ mg L}^{-1}$  streptomycin, aligning with concentrations reported by Sanz et al. (1996), where methanogenesis was not significantly affected. Therefore, 5 % v/v concentration was considered as a balanced and cautious upper threshold.

Antibiotics initially delayed citrate degradation; however, a late-stage decline in citrate levels observed after day 30 suggests microbial adaptation. Prolonged antibiotic exposure likely facilitated the selection of antibiotic-resistant strains or triggered alternative metabolic pathways that eventually capable of citrate degradation, in line with antibiotic resistance literature (Peterson and Kaur, 2018). This adaptive response highlights the limitations of prolonged antibiotic usage and

underscores the need for transient or alternative strategies to maintain ligand stability in  $\text{Fe}^0$ -assisted anaerobic digestion.

### 3.4. The role of CA in methanogenesis stage

An experiment was conducted comprising 6 different conditions involving AGS,  $\text{NaHCO}_3$  and  $\text{Fe}^0$  (30 mM,  $1.68 \text{ g L}^{-1}$ ), CA and antibiotics with the corresponding control for each case, as detailed in Section 2.2.4.

Fig. 6a and b illustrates the production of  $\text{CH}_4$  and  $\text{CO}_2$  over a 50-day period. The highest  $\text{CH}_4$  production occurred in the AGS-Bic-CA-Fe and AGS-Bic-CA samples. A rapid increase in methane was noted in these samples on day 4, reaching 27 ml  $\text{CH}_4$ , peaking at 40 ml by day 7, and stabilizing around 40 ml until day 50 (Fig. 6a). These observations can be attributed to CA degradation after four days (Fig. 6d), which provided a substantial substrate for bacterial and subsequent methanogenic activity. It is crucial to highlight that no significant difference was observed in net methane production between the two samples (AGS-Bic-CA-Fe and AGS-Bic-CA) (Fig. 6c), suggesting that the contribution of  $\text{Fe}^0$  in the Bic-CA solution is negligible, likely due to relatively low concentration of  $\text{Fe}^0$  (30 mM,  $1.68 \text{ g L}^{-1}$ ) and the formation of the passivation layer ( $\text{FeCO}_3$ ) on the surface of  $\text{Fe}^0$ , resulting from the high  $\text{CO}_2$  concentration in the system.

After 50 days, both AGS-Bic and AGS-Bic-Fe samples produced

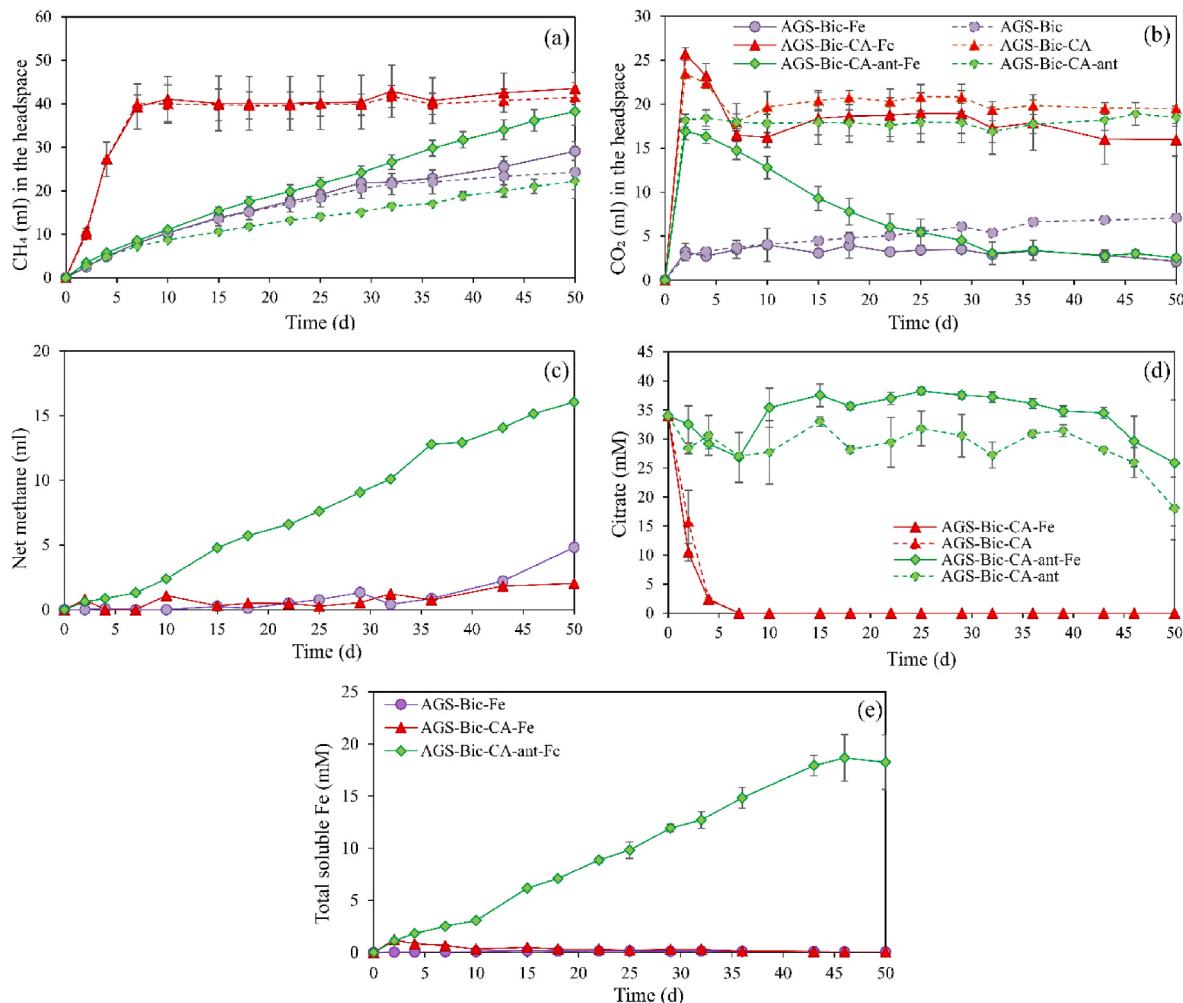


**Fig. 6.** (a)  $\text{CH}_4$  (ml) production over time, (b)  $\text{CO}_2$  (ml) in the headspace over time, (c) net methane (ml) production between AGS-Bic-CA-ant-Fe and AGS-Bic-CA-ant (—◆—), AGS-Bic-Fe and AGS-Bic (—●—), AGS-Bic-CA-Fe and AGS-Bic-CA (—▲—), (d) citrate (mM) degradation over time, and (e) total soluble Fe (mM) over time for the  $\text{Fe}^0$  – amended samples. The net methane production represents the difference between each sample and its control, with no Fe. Each assay was conducted using 0.33g VS of inoculum.

approximately 26 ml of CH<sub>4</sub>, as shown in Fig. 6a. Importantly, as Fig. 6c shows, net methane production between the comparable samples AGS-Bic and AGS-Bic-Fe was 4.8 ml, which implies that the functionality of 30 mM Fe<sup>0</sup> is inactivated under carbonate conditions. On the other hand, the sample with the addition of CA, antibiotics and Fe<sup>0</sup> (AGS-Bic-CA-ant-Fe) showed a steadily increasing rate of CH<sub>4</sub> production, reaching 38 ml on day 50. In contrast, the corresponding sample without the addition of Fe<sup>0</sup> (AGS-Bic-CA-ant) presented a slower rate of methane, reaching 22 ml of CH<sub>4</sub> over the same period. These results indicate a net methane increase of 16 ml (Fig. 6c – green line), which is attributed to the addition of iron in the AGS-Bic-CA-ant-Fe sample. In this case, the presence of antibiotics inhibited bacterial growth, thereby preventing the biodegradation of CA as Fig. 6d shows. Notably as Fig. 6c shows, only the system containing the antibiotic demonstrated a significant difference compared to its corresponding control (under the same conditions but without Fe<sup>0</sup>). As previously noted, the other two systems—(a) AGS-Bic-CA-Fe with its corresponding control AGS-Bic-CA, and (b) AGS-Bic-Fe with its corresponding control AGS-Bic—did not exhibit any substantial difference in net methane generation. These results highlight the positive impact of antibiotic addition in the system containing citric acid, AGS, and Fe<sup>0</sup>, and emphasize the importance of appropriate controls when using chelating agents such as CA in these systems.

In the system AGS-Bic-CA-ant-Fe, CA remained soluble over time and was able to facilitate iron activity, leading to enhanced methane production (Fig. 6d). Notably, continuous increase in total soluble Fe was observed (Fig. 6e), indicating effective Fe-chelation by citrate, which prevented siderite precipitation and maintained iron bioavailability. In contrast, in the AGS-Bic-CA-Fe sample, citrate was rapidly depleted within the first few days, and soluble iron levels remained low throughout the experiment, suggesting rapid biodegradation of CA and limited chelation efficiency (Fig. 6d and e). However, after 46 days, a noticeable decrease in citrate concentration was also observed across the AGS-Bic-CA-ant-Fe and AGS-Bic-CA-ant samples (Fig. 6d), which may be attributed to bacteria adaptation on this environment, leading to citrate biodegradation.

Significant CO<sub>2</sub> production was observed on day 2 in samples containing CA and bicarbonate ions (HCO<sub>3</sub><sup>-</sup>) (Fig. 6b). This rapid increase results from the reaction between CA and NaHCO<sub>3</sub>, as described in equation (4). Notably, the samples AGS-Bic-CA-Fe and AGS-Bic-CA (Fig. 6b - red lines) exhibit a pronounced spike in CO<sub>2</sub> production, reaching approximately 25 ml on the 2<sup>nd</sup> day. This is followed by a gradual decrease at 17 ml on day 7, which remained stable for the rest of the experiment (Fig. 6b). This is attributed to the fact that CA is biodegraded by bacteria to CO<sub>2</sub>, which is leading to the accumulation of carbon dioxide in the system. The same trend is observed in the case where CA and antibiotics (AGS-Bic-CA-ant) were introduced. In contrast, CO<sub>2</sub> volume in sample AGS-Bic-CA-ant-Fe decreased over time reaching 2.5 ml on day 50 (Fig. 6b). This trend indicates that the presence of Fe<sup>(0)</sup> facilitates the enrichment of hydrogenotrophic methanogens, providing a favorable environment for their growth, leading to the reduction of CO<sub>2</sub> in conjunction with the production of CH<sub>4</sub> via hydrogenotrophic pathway. As for the samples without the presence of CA (AGS-Bic, AGS-Bic-Fe, purple lines), CO<sub>2</sub> in the headspace remained stable at lower volume levels.

Initial and final pH values of the tested samples are presented in Table 1. As the initial pH of the solutions was not maintained at a desired pH value, this allowed to observe the effect of CA on pH levels. Samples containing CA (AGS-Bic-CA-Fe, AGS-Bic-CA, AGS-Bic-CA-ant-Fe, AGS-Bic-CA-ant) exhibited an initial pH value of approximately 6.2, whereas the samples without the addition of CA (AGS-Bic-Fe, AGS-Bic) had a higher initial pH of around 8.5. The final pH of the Fe<sup>0</sup>-containing samples was higher than that of the corresponding control samples (without Fe<sup>0</sup> addition). According to equation (3), Fe<sup>0</sup> anaerobic corrosion under carbonate environment, leads to the consumption of H<sup>+</sup>, which promotes alkalinity. The presence of CA appears to favor the pH in methanogenesis (final pH range 7–7.8), by potentially acting as a

**Table 1**

Initial and final pH values, final Fe<sup>2+</sup>, Fe<sup>3+</sup>, and total soluble iron concentrations (mM) measured in the liquid phase for Fe<sup>0</sup>-amended and control samples. (Initial Fe<sup>0</sup> used: 30 mM).

Sample	pH initial	pH final	Fe <sup>2+</sup> (mM)	Fe <sup>3+</sup> (mM)	Total soluble Fe (mM)
AGS-Bic-Fe	8.48	8.91	0.01	0.04	0.05
AGS-Bic	8.48	7.73	0.00	0.00	0.00
AGS-Bic-CA-Fe	6.26	7.42	0.02	0.05	0.07
AGS-Bic-CA	6.26	7.15	0.00	0.00	0.00
AGS-Bic-CA-ant-Fe	6.21	7.80	12.59	5.64	18.23
AGS-Bic-CA-ant	6.21	6.96	0.00	0.00	0.00

buffer, which is beneficial for methanogens that function optimally within a pH range of 6.5–7.5.

The final concentration of iron species (Fe<sup>2+</sup> and Fe<sup>3+</sup>) and total soluble iron of the Fe<sup>0</sup>-amended samples (AGS-Bic-Fe, AGS-Bic-CA-Fe, AGS-Bic-CA-ant-Fe) are shown in Table 1. Notably, the AGS-Bic-CA-Fe-ant sample demonstrates a continuous increase in soluble iron levels over time, reaching 18.23 mM, by day 50, of which 12.59 mM corresponds to ferrous ion and 5.46 to ferric ion. Given that the initial iron concentration was 30 mM, it is suggested that over 50 % of the iron remained in its soluble form, forming a complex with citrate, thus, preventing the precipitation of Fe<sup>2+</sup> to FeCO<sub>3</sub>. In contrast, the other two samples AGS-Bic-Fe and AGS-Bic-CA-Fe, maintain consistently low levels of soluble iron throughout the experiment, indicating the precipitation of iron (Table 1). Thus, the presence of antibiotics plays a critical role in preventing the biodegradation of citric acid, thereby sustaining the iron complex and preventing the early formation of passivation layer.

Studies (Khemkha et al., 2024; Ma et al., 2018; Vyrides et al., 2018) focused on the biotransformation of CO<sub>2</sub> to CH<sub>4</sub> have demonstrated that Fe<sup>(0)</sup> positively contribute to the conversion process, due to the generation of H<sub>2</sub>, which is promoted from the iron oxidation. For instance, Ma et al. (2018) used 716 mM Fe<sup>0</sup> to achieve a methane production rate >61 μmol L<sup>-1</sup> d<sup>-1</sup>, while the corresponding controls without Fe<sup>0</sup> exhibited methane production rates of less than 0.12 μmol L<sup>-1</sup> d<sup>-1</sup>. However, in the present study, Fe<sup>0</sup> did not appear to significantly contribute to the bioconversion of CO<sub>2</sub> to CH<sub>4</sub>, as the net methane production were low (Fig. 6c - lines red and purple). This outcome is likely due to the lower initial Fe<sup>0</sup> concentration of 30 mM used in our experiments, compared with studies that have been used higher concentrations of iron (Khemkha et al., 2024; Ma et al., 2018; Vyrides et al., 2018). Interestingly, when CA and antibiotics were introduced into the system, net methane was notably enhanced (Fig. 6c – green line), suggesting that the limitation of lower Fe<sup>0</sup> concentrations can overcome, potentially by maintaining iron solubility, with CA as a ligand. By preventing iron precipitation, continuous iron oxidation is facilitated, enabling sustained electron release that enhances the microbial reduction of CO<sub>2</sub> to CH<sub>4</sub>.

### 3.4.1. Future sustainable strategies for enhancing citrate stability and performance

Hendriks et al. (2018) reviewed CA, nitrilotriacetic acid (NTA), and EDTA as potential chelators in anaerobic digestion. They reported that CA is effective above pH 4.76 but readily biodegradable, a finding that aligns with observations made in the current study. In contrast, NTA exhibits greatest stability and is compatible with methanogenic microorganisms, while EDTA, despite having the highest chelating strength, may inhibit methanogenesis due to its tendency to complex essential metal ions necessary for microbial activity. Liu et al. (2019) demonstrated that the addition of EDTA improved methane production by approximately 5.8 % and increased water-soluble iron fractions by

approximately 1.5 times compared to  $\text{Fe}^{2+}$  alone; however, the strong complexation by EDTA occasionally limited metal bioavailability. Additionally, Zhang et al. (2021) reported that NTA addition enhanced methane yields by up to 25 % and maintained higher soluble metal concentrations, highlighting its advantage over EDTA in maintaining metal availability.

Table 2 highlights that the stability constant ( $\log K$ ) for the  $\text{Fe}^{2+}$ -citrate complexes is significantly 2 to 3 orders of magnitude lower than those of EDTA and NTA. Nevertheless, CA presents distinct advantages in terms of cost, availability, and environmental compatibility. Its price is approximately two to three times less expensive than that of NTA and EDTA, making it a considerably more economical option for large-scale applications. Moreover, the renewable sourcing potential of CA from citrus fruits enhances its sustainability profile. Considering these factors, CA was selected as the ligand for the Fe–CO<sub>2</sub> system, with antibiotics employed to temporarily suppress microbial activity and preserve the chelation function of citrate.

As a strategy to prevent citrate biodegradation and maintain its performance, antibiotics were found to be beneficial. However, this approach is not practical on a larger scale due to concerns regarding environmental impact, regulatory constraints, and the potential for antimicrobial resistance. Future research should explore alternative strategies, such as optimizing citrate concentration, using structurally modified ligands resistant to biodegradation, or developing biocompatible inhibitors that selectively prevent citrate degradation without affecting methanogenic activity.

Additionally, a potential strategy for future studies could involve the controlled exposure of CA as a ligand for a limited duration (e.g., less than 12 h) (Supplementary Fig. 2). This approach would allow CA to effectively prevent iron precipitation while minimizing its biodegradation, as previous findings indicate that citrate degradation typically begins after 12 h (Supplementary Fig. 2). By optimizing the timing of CA introduction and removal, it may be possible to maintain iron solubility and enhance methane production without relying on antibiotics. This strategy could be implemented in systems such as sequencing batch reactors (SBR) or anaerobic membrane bioreactors (AnMBR), where the microbial biomass is retained while allowing controlled, short-term exposure of citrate to the liquid phase.

This process offers compelling environmental and economic advantages by simultaneously enabling CO<sub>2</sub> sequestration and methane

**Table 2**  
Comparison of  $\text{Fe}^{2+}/\text{Fe}^{3+}$  stability constants, biodegradability, and cost of selected ligands.

Ligand	Fe <sup>2+</sup> Stability Constant - $\log K$	Fe <sup>3+</sup> Stability Constant - $\log K$	Biodegradability	Price (€/ton)
CA	5.89 <sup>1</sup>	13.13 <sup>1</sup>	Readily biodegradable under anaerobic conditions; rapidly metabolized and does not persist in biogas systems.	600–750
EDTA	16.01 <sup>1</sup>	27.66 <sup>1</sup>	Poorly biodegradable under anaerobic conditions; may inhibit methanogenesis by outcompeting cell-surface sites and binding $\text{Ca}^{2+}$ / $\text{Mg}^{2+}$ .	1530 - 1700
NTA	10.18 <sup>1</sup>	17.82 <sup>1</sup>	Moderately biodegradable under anaerobic conditions; more stable than citric acid but degrades over time without acutely inhibiting anaerobic digestion.	1800 - 2000

<sup>1</sup> (Hudson et al., 2022).

generation, converting two low-value inputs—carbon dioxide and metallic iron—into a renewable energy carrier. The formation of  $\text{FeCO}_3$  not only contributes to long-term CO<sub>2</sub> immobilization but also presents opportunities for material recovery and reuse. Moreover, replacing high-purity iron with scrap iron could significantly reduce costs and improve sustainability. Previous studies (Andronikou et al., 2022; Charalambous et al., 2023; Menikea et al., 2020) have demonstrated the successful use of scrap iron in anaerobic digestion processes, achieving enhanced methane production. However, these results were obtained using high concentrations of scrap iron (>25 g L<sup>-1</sup>). Further research is needed to assess the effects of scrap iron dosage, potential pre-treatment methods (e.g., ball milling), and associated costs, in order to determine the overall feasibility and performance of scrap iron in practical applications.

### 3.5. Microbial profile

Fig. 7a shows the microbial community composition at the phylum and genus levels for the control AGS and BES-treated samples (Bic-CA-BES and Bic-CA-Fe-BES) after 14 days of incubation with citric acid. *Firmicutes*, *Desulfobacterota*, and *Spirochaetota* were the dominant phyla in CA biodegradation, with relative abundances in the Bic-CA-Fe-BES sample at 33.8 %, 17.5 %, and 8.2 %, respectively.  $\text{Fe}^0$  enhanced *Firmicutes* and *Desulfobacterota*, increasing their relative abundances by 1.44 and 1.5 times compared to the Bic-CA-BES sample. *Firmicutes* play a key role in the breakdown of complex organic matter, as they can convert macromolecular organic substances into smaller molecules, such as acetic acid, while simultaneously generating electrons, thereby facilitating CA degradation (Guo et al., 2023). Their dominance in high-CA wastewater MFC reactors further highlights their importance in CA degradation (Zhang et al., 2021). The homoacetogenic bacteria (Groher and Weuster-Botz, 2016; Zhu et al., 2020), *Terrisporobacter* sp. was significantly more abundant in the presence of Bic-CA-Fe-BES (7.9 %) compared to the other two systems due to the utilization of CO<sub>2</sub> and H<sub>2</sub> in the presence of  $\text{Fe}^0$ . Moreover, *Geosporobacter* genus was more abundant in the Bic-CA-Fe-BES (7.8 %) compared to the other two samples, suggesting its potential involvement in citric acid utilization. In the systems with citric acid, *Syntrophobacter* genus which belongs to *Desulfobacterota* phylum, increased 4 % compared to the control (Fig. 7a), and this genus can potentially facilitate the utilization of propionic acid in those systems. *Exilispira* genus belongs to phylum *Spirochaetota*, showed high relative abundance (21.9 %) in Bic-CA-BES, compared to Bic-CA-Fe-BES (5.7 %). *Exilispira* is an acetate-oxidizing bacteria, indicating that after 14 days of incubation, part of acetic acid was probably utilized by this genus.

Fig. 7b demonstrates the relative abundances of microbial communities at the phylum and genus levels in the control AGS (original AGS) and the tested samples (based on Section 3.4.) at the end of the incubation period (50 days). The hydrogenotrophic methanogen *Methanobacterium* is a key archaeal group responsible for converting CO<sub>2</sub>/H<sub>2</sub> to CH<sub>4</sub> under mesophilic conditions, whereas *Methanosaeta* genus, primarily relies on the utilization of acetic acid for methanogenesis. In the Control reactor, *Methanosaeta* was the most dominant methanogenic genus (14.2 %), followed by *Methanobacterium* (9.0 %). Comparing the Bic and Bic-Fe samples, *Methanobacterium* showed a higher relative abundance in Bic-Fe (23.9 %) than in Bic (14.7 %), while *Methanosaeta* was detected exclusively in the Bic sample (Fig. 7b). In a previous study, *Methanobacterium* was found to be the dominant and contributed significantly to the biomethanation of CO<sub>2</sub> in the presence of  $\text{Fe}^0$  (Dong et al., 2022). By comparing Bic-CA and Bic-CA-Fe with their corresponding samples containing antibiotics, *Methanobacterium* exhibited a higher relative abundance in the samples with antibiotics, most likely due to the fact that acetocalstic methanogens were more prone to antibiotic inhibition. In the Bic-CA and Bic-CA-Fe samples, the relative abundance of *Methanosaeta* increased to 21.5 % and 14.6 %, respectively, likely due to the utilization of acetic acid derived from the

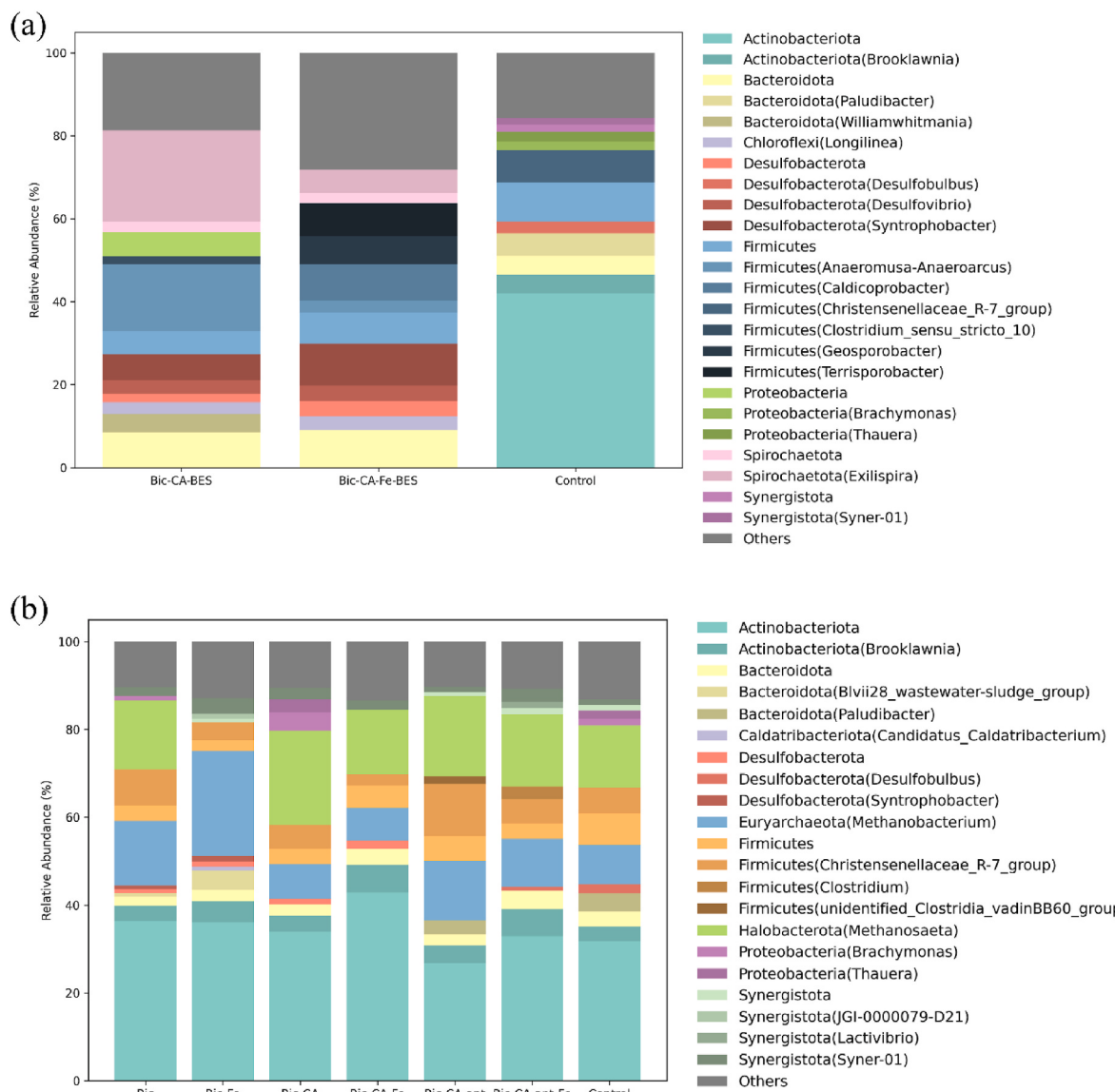


**Fig. 7.** Relative abundances of the microbial community obtained at the end of the incubation time of (a) control (original AGS) and samples treated with BES and (b) control (original AGS) and tested samples – based on section 3.4. Legends represent phylum (genus).

degradation of CA. Interestingly, a similar trend was also observed in the sample exposed to Bic,  $\text{Fe}^0$ , and antibiotics, with relative abundance of *Methanosaeta* at 18.3 % for Bic-CA-ant and 16.4 % for Bic-CA-ant-Fe (Fig. 7b). This can be attributed to the fact that samples were withdrawn after 50 days, providing sufficient time for the citric acid to biodegrade (as shown before) and generate acetic acid, which could then be utilized by *Methanosaeta* as a substrate. Notably, this observation aligns with the increased relative abundance of *Firmicutes*, suggesting that CA degradation during the later stages of the incubation time, created favorable conditions for *Firmicutes* to thrive. Interestingly, in the system containing  $\text{Fe}^0$ , the relative abundance of *Syner-01* was higher compared to systems without  $\text{Fe}^0$ . *Syner-01* may facilitate the syntrophic utilization of acetic acid, and the conductive nature of  $\text{Fe}^0$  likely supports its presence. The study by Zhu et al. (2023) demonstrated that the addition of conductive materials, such as granular activated carbon (GAC), biochar, and magnetite, significantly enhanced the anaerobic digestion performance of hydrothermal liquefaction aqueous phase (HTL-AP) by improving methane production, organic matter degradation, and microbial enrichment. *Syner-01* played a critical role in syntrophic acetate and amino acid oxidation, supporting acetoclastic methanogenesis and contributing to sulfate removal. Its electroactive

nature suggests its involvement in DIET with methanogens, enhancing metabolic cooperation and digestion efficiency. These findings highlight the potential of conductive materials and the syntrophic role of *Syner-01* in improving anaerobic digestion systems. These shifts suggest that CA and antibiotics influenced not only substrate availability but also methanogenic pathway dominance.

The enrichment of *Methanobacterium* in  $\text{Fe}^0$  and antibiotic-treated systems points to enhanced hydrogenotrophic methanogenesis, likely due to sustained  $\text{H}_2$  availability and reduced competition from *Methanosaeta*, which appeared more sensitive to antibiotics. In contrast, CA-amended systems favored *Methanosaeta* due to acetate accumulation from CA degradation. The presence of *Syner-01* in  $\text{Fe}^0$  systems may indicate DIET activity, facilitated by  $\text{Fe}^0$ 's conductive properties, supporting syntrophic acetate oxidation and further methane production.

#### 4. Conclusions

This study presents a promising approach to enhance  $\text{CO}_2$ -to- $\text{CH}_4$  bioconversion using AGS with  $\text{Fe}^0$ . CA was evaluated as a ligand during methanogenesis to prevent  $\text{Fe}^{2+}$  precipitation as  $\text{FeCO}_3$ . Batch experiments employing with AGS and  $\text{NaHCO}_3$  with CA, revealed that the

formed citrate biodegraded to acetic acid and CO<sub>2</sub> gas. To maintain the beneficial effects of citric acid while preventing its biodegradation, the addition of antibiotics was examined as a research tool. The underlying assumption was that hydrogenotrophic methanogens, which utilize H<sub>2</sub> and CO<sub>2</sub>, would remain unaffected by the antibiotics, while bacteria responsible for citrate biodegradation would be inhibited. The introduction of 5 % v/v antibiotics in the system effectively prevented citrate biodegradation, indicating the formation of a stable Fe<sup>2+</sup>- citrate complex and thereby inhibiting the formation of FeCO<sub>3</sub> passivation layer. Methane production was notably enhanced in the sample with NaHCO<sub>3</sub>, citric acid, antibiotics, and Fe<sup>0</sup>, reaching 38 ml by day 50, whereas the corresponding sample without iron produced only 22 ml, leading to a net methane production of 16 ml. By contrast, samples with NaHCO<sub>3</sub> in the presence and absence of Fe<sup>0</sup>, produced 29.1 ml and 24.3 ml CH<sub>4</sub>, respectively, after 50 days, yielding a net methane production of 4.8 ml. The results suggest that CA positively influenced methane production, primarily by maintaining iron in a soluble state and preventing its precipitation, thereby facilitating continuous iron oxidation and sustained electron release, which supports the microbial reduction of CO<sub>2</sub> to CH<sub>4</sub>.

Although antibiotics were effective in this context, they are not practical for large-scale application. Future strategies could involve optimizing ligand exposure time (e.g., <12 h) or exploring alternative bio-compatible chelators. Overall, this proof-of-concept study emphasizes the dual role of Fe<sup>0</sup> in CO<sub>2</sub> sequestration and renewable methane production and supports further development of ligand-assisted approaches to mitigate passivation and enhance system performance.

#### CRediT authorship contribution statement

**Despina Constantinou:** Writing – review & editing, Writing – original draft, Validation, Methodology, Investigation, Formal analysis, Data curation, Conceptualization. **Ioannis Vyrideres:** Writing – review & editing, Visualization, Supervision, Project administration, Methodology, Formal analysis, Conceptualization.

#### Declaration of competing interest

The authors declare the following financial interests/personal relationships which may be considered as potential competing interests: Ioannis Vyrideres reports was provided by Cyprus University of Technology. Ioannis Vyrideres reports a relationship with Cyprus University of Technology that includes: employment. Ioannis Vyrideres reports was provided by Cyprus University of Technology Department of Chemical Engineering. Ioannis Vyrideres reports a relationship with Cyprus University of Technology Department of Chemical Engineering that includes: employment. Ioannis Vyrideres reports a relationship with Cyprus University of Technology that includes: employment. No any additional relationships or activities to declare If there are other authors, they declare that they have no known competing financial interests or personal relationships that could have appeared to influence the work reported in this paper. If there are other authors, they declare that they have no known competing financial interests or personal relationships that could have appeared to influence the work reported in this paper.

#### Appendix A. Supplementary data

Supplementary data to this article can be found online at <https://doi.org/10.1016/j.jenvman.2025.126641>.

#### Data availability

Data will be made available on request.

#### References

- Andronikou, M., Lytras, N., Chrysanthou, G., Koutsokeras, L., Constantinides, G., Stylianou, M., Agapiou, A., Vyrideres, I., 2022. Biogas upgrading to methane and removal of volatile organic compounds in a system of zero-valent iron and anaerobic granular sludge. *Environ. Sci. Pollut. Res.* 29, 87245–87256. <https://doi.org/10.1007/s11356-022-217505>.
- Baek, G., Kim, J., Lee, C., 2019. A review of the effects of iron compounds on methanogenesis in anaerobic environments. *Renew. Sustain. Energy Rev.* 113, 109282. <https://doi.org/10.1016/j.rser.2019.109282>.
- Cai, Y., Hu, K., Zheng, Z., Zhang, Y., Guo, S., Zhao, X., Cui, Z., Wang, X., 2019. Effects of adding EDTA and Fe<sup>2+</sup> on the performance of reactor and microbial community structure in two simulated phases of anaerobic digestion. *Bioresour. Technol.* 275, 183–191. <https://doi.org/10.1016/j.biortech.2018.12.050>.
- Charalambous, P., Constantinou, D., Samanides, C.G., Vyrideres, I., 2023. Enhancing biogas production from cheese whey using zero-valent iron: a comparative analysis of batch and semi-continuous operation modes. *J. Environ. Chem. Eng.* 11. <https://doi.org/10.1016/j.jece.2023.111278>.
- Cheng, J., Dong, H., Zhang, H., Yuan, L., Li, H., Yue, L., Hua, J., Zhou, J., 2020. Improving CH<sub>4</sub> production and energy conversion from CO<sub>2</sub> and H<sub>2</sub> feedstock gases with mixed methanogenic community over Fe nanoparticles. *Bioresour. Technol.* 314, 123799. <https://doi.org/10.1016/j.biortech.2020.123799>.
- Constantinou, D., Samanides, C.G., Koutsokeras, L., Constantinides, G., Vyrideres, I., 2023. Hydrogen generation by soluble CO<sub>2</sub> reaction with zero-valent iron or scrap iron and the role of weak acids for controlling FeCO<sub>3</sub> formation. *Sustain. Energy Technol. Assessments* 56, 103061. <https://doi.org/10.1016/j.seta.2023.103061>.
- Dias, Y.R., Perez-Lopez, O.W., 2021. CO<sub>2</sub> conversion to methane using Ni/SiO<sub>2</sub> catalysts promoted by Fe, Co and Zn. *J. Environ. Chem. Eng.* 9, 104629. <https://doi.org/10.1016/j.jece.2020.104629>.
- Dong, D., Aleta, P., Zhao, X., Choi, O.K., Kim, S., Lee, J.W., 2019. Effects of nanoscale zero valent iron (nZVI) concentration on the biochemical conversion of gaseous carbon dioxide (CO<sub>2</sub>) into methane (CH<sub>4</sub>). *Bioresour. Technol.* 275, 314–320. <https://doi.org/10.1016/j.biortech.2018.12.075>.
- Dong, D., Kyung Choi, O., Woo Lee, J., 2022. Influence of the continuous addition of zero valent iron (ZVI) and nano-scaled zero valent iron (nZVI) on the anaerobic biomethanation of carbon dioxide. *Chem. Eng. J.* 430. <https://doi.org/10.1016/j.cej.2021.132233>.
- Energy Institute, 2023. *Statistical Review of World Energy 2023. BP Energy Outlook 2023*.
- Fang, W., Liu, X., Zhang, J., Hou, H., Yue, Y., Qian, G., 2023. Dual mechanisms of Ni and Si sludge-derived catalyst for catalytic methanation with high CO<sub>2</sub> conversion and CH<sub>4</sub>selectivity. *J. Environ. Chem. Eng.* 11, 109341. <https://doi.org/10.1016/j.jece.2023.109341>.
- Feng, J., Zheng, Y., Ma, W., Ihsan, A., Hao, H., Cheng, G., Wang, X., 2023. Multitarget antibacterial drugs: an effective strategy to combat bacterial resistance. *Pharmacol. Ther.* 252, 108550. <https://doi.org/10.1016/j.pharmthera.2023.108550>.
- Gámez, V.M., Sierra-Alvarez, R., Waltz, R.J., Field, J.A., 2009. Anaerobic degradation of citrate under sulfate reducing and methanogenic conditions. *Biodegradation* 20, 499–510.
- Gao, T., Xia, L., Zhang, H., Tawfik, A., Meng, F., 2024. Fe<sup>0</sup>-dependent carbon dioxide reduction to methane via diverse electron transfer pathway in methanogenic community. *Cell Reports Sustain* 1, 100019. <https://doi.org/10.1016/j.crsus.2024.100019>.
- Groher, A., Weuster-Botz, D., 2016. Comparative reaction engineering analysis of different acetogenic bacteria for gas fermentation. *J. Biotechnol.* 228, 82–94. <https://doi.org/10.1016/j.biote.2016.04.032>.
- Guo, W., Chen, Y., Cui, L., Xu, N., Wang, M., Sun, Y., Yan, Y., 2023. Nano-Hydroxyapatite/carbon nanotube: an excellent anode modifying material for improving the power output and diclofenac sodium removal of microbial fuel cells. *Bioelectrochemistry* 154, 108523. <https://doi.org/10.1016/j.bioelechem.2023.108523>.
- He, Z.W., Zou, Z.S., Ren, Y.X., Tang, C.C., Zhou, A.J., Liu, W., Wang, L., Li, Z., Wang, A., 2022. Roles of zero-valent iron in anaerobic digestion: mechanisms, advances and perspectives. *Sci. Total Environ.* 852, 158420. <https://doi.org/10.1016/j.scitotenv.2022.158420>.
- Hendriks, A.T.W.M., van Lier, J.B., de Kreuk, M.K., 2018. Growth media in anaerobic fermentative processes: the underestimated potential of thermophilic fermentation and anaerobic digestion. *Biotechnol. Adv.* 36, 1–13. <https://doi.org/10.1016/j.biotechadv.2017.08.004>.
- Hudson, J.M., Luther, G.W., Chin, Y.P., 2022. Influence of organic ligands on the redox properties of Fe(II) as determined by mediated electrochemical oxidation. *Environ. Sci. Technol.* 56, 9123–9132. <https://doi.org/10.1021/acs.est.2c01782>.
- Jiang, H., Hao, W., Li, Y., Zhou, H., 2022. Biological methanation of H<sub>2</sub> and CO<sub>2</sub> in a continuous stirred tank reactor. *J. Clean. Prod.* 370, 133518. <https://doi.org/10.1016/j.jclepro.2022.133518>.
- Khemkhao, M., Domrongpokkaphan, V., Nuchdang, S., Phalakornkule, C., 2024. Chemical and biological effects of zero-valent iron (ZVI) concentration on in-situ production of H<sub>2</sub> from ZVI and biocconversion of CO<sub>2</sub> into CH<sub>4</sub> under anaerobic conditions. *Environ. Res.* 256, 119230. <https://doi.org/10.1016/j.envres.2024.119230>.
- Kumar, S., Dagar, S.S., Puniya, A.K., 2012. Isolation and characterization of methanogens from rumen of Murrah buffalo. *Ann. Microbiol.* 62, 345–350. <https://doi.org/10.1007/s13213-011-0268-8>.
- Lins, P., Reitschuler, C., Ilmer, P., 2015. Impact of several antibiotics and 2-bromoethanesulfonate on the volatile fatty acid degradation, methanogenesis and

- community structure during thermophilic anaerobic digestion. *Bioresour. Technol.* 190, 148–158. <https://doi.org/10.1016/j.biortech.2015.04.070>.
- Liu, Y., Kang, X., Cheng, H., 2019. Enhanced anaerobic performances of kitchen wastes in a semi-continuous reactor by EDTA improving the water-soluble fraction of Fe. *Processes* 7. <https://doi.org/10.3390/pr7060351>.
- Liu, Y., Wang, Q., Zhang, Y., Ni, B.J., 2015. Zero valent iron significantly enhances methane production from waste activated sludge by improving biochemical methane potential rather than hydrolysis rate. *Sci. Rep.* 5, 1–6. <https://doi.org/10.1038/srep08263>.
- Ma, L., Zhou, L., Mbadinga, S.M., Gu, J.D., Mu, B.Z., 2018. Accelerated CO<sub>2</sub> reduction to methane for energy by zero valent iron in oil reservoir production waters. *Energy* 147, 663–671. <https://doi.org/10.1016/j.energy.2018.01.087>.
- Meng, Q., Bin, He, Z.W., Yang, W., Li, W.T., Tang, C.C., Zhou, A.J., Ren, Y.X., Liu, W., Li, Z., Wang, A., 2024. Roles and fates of antibiotics in anaerobic digestion of waste activated sludge insights to pro- and re-duction of antibiotic resistance genes. *Chem. Eng. J.* 500, 156633. <https://doi.org/10.1016/j.cej.2024.156633>.
- Menikea, K.K., Kyprianou, A., Samanides, C.G., Georgiou, S.G., Koutsokeras, L., Constantinides, G., Vyrides, I., 2020. Anaerobic granular sludge and zero valent scrap iron (ZVSI) pre-treated with green tea as a sustainable system for conversion of CO<sub>2</sub> to CH<sub>4</sub>. *J. Clean. Prod.* 268, 121860. <https://doi.org/10.1016/j.jclepro.2020.121860>.
- Palacios, P.A., Francis, W.R., Rotaru, A.E., 2021. A win-loss interaction on Fe<sup>0</sup> between methanogens and acetogens from a climate Lake. *Front. Microbiol.* 12, 638282. <https://doi.org/10.3389/fmicb.2021.638282>.
- Peterson, E., Kaur, P., 2018. Antibiotic resistance mechanisms in bacteria: relationships between resistance determinants of antibiotic producers, environmental bacteria, and clinical pathogens. *Front. Microbiol.* 9, 2928. <https://doi.org/10.3389/fmicb.2018.02928>.
- Quintans, N.G., Blancato, V., Repizo, G., Magni, C., Lopez, P., 2008. Citrate metabolism and aroma compound production in lactic acid bacteria. *Res. Signpost* 37, 65–88.
- Sanz, J.L., Rodriguez, N., Amils, R., 1996. The action of antibiotics on the anaerobic digestion process. *Appl. Microbiol. Biotechnol.* 46, 587–592. <https://doi.org/10.1007/s002530050865>.
- Stookey, L.L., 1970. Ferrozine-A new spectrophotometric reagent for iron. *Anal. Chem.* 42, 779–781. <https://doi.org/10.1021/ac60289a016>.
- Tian, T., Yu, H.Q., 2020. Iron-assisted biological wastewater treatment: synergistic effect between iron and microbes. *Biotechnol. Adv.* 44. <https://doi.org/10.1016/j.biotechadv.2020.107610>.
- Viswanath, P., Nand, K., 1989. Influence of penicillin on the stabilization of anaerobic digestion of rain tree kernels for methane generation. *J. Ferment. Bioeng.* 68, 154–156. [https://doi.org/10.1016/0922-338X\(89\)90067-6](https://doi.org/10.1016/0922-338X(89)90067-6).
- Vyrides, I., Andronikou, M., Kyprianou, A., Modic, A., Filippeti, A., Yiakoumis, C., Samanides, C.G., 2018. CO<sub>2</sub> conversion to CH<sub>4</sub> using zero valent iron (ZVI) and anaerobic granular sludge: optimum batch conditions and microbial pathways. *J. CO<sub>2</sub> Util.* 27, 415–422. <https://doi.org/10.1016/j.jcou.2018.08.023>.
- Wang, F., Zou, Z., He, Z., Tang, C., Zhou, A., 2023. Revealing methane production potential from waste activated sludge through citric acid-assisted hydrogen corrosion of zero valent iron. *Chem. Eng. J.*, 145195. <https://doi.org/10.1016/j.cej.2023.145195>.
- Xiao, L., Wang, Y., Lichtfouse, E., Li, Z., Kumar, P.S., Liu, J., Feng, D., Yang, Q., Liu, F., 2021. Effect of antibiotics on the microbial efficiency of anaerobic digestion of wastewater: a review. *Front. Microbiol.* 11, 611613. <https://doi.org/10.3389/fmcb.2020.611613>.
- Xu, H., Giwa, A.S., Wang, C., Chang, F., Yuan, Q., Wang, K., Holmes, D.E., 2017. Impact of antibiotics pretreatment on bioelectrochemical CH<sub>4</sub> production. *Sustain. Chem. Eng.* 5, 8579–8586. <https://doi.org/10.1021/acssuschemeng.7b00923>.
- Zabranska, J., Pokorna, D., 2018. Bioconversion of carbon dioxide to methane using hydrogen and hydrogenotrophic methanogens. *Biotechnol. Adv.* 36, 707–720. <https://doi.org/10.1016/j.biotechadv.2017.12.003>.
- Zandt, M.H. in't, Kip, N., Frank, J., Jansen, S., van Veen, J.A., Jetten, M.S.M., Wetle, C. U., 2019. High-Level Abundances of Methanoaerobiales and Syntrophobacterales May Help to Prevent Corrosion of Metal Sheet Piles, vol. 85. <https://doi.org/10.1128/AEM.01369-19>.
- Zhang, M., Fan, Z., Hu, Z., Luo, X., 2021. Enhanced anaerobic digestion with the addition of chelator-nickel complexes to improve nickel bioavailability. *Sci. Total Environ.* 759, 143458. <https://doi.org/10.1016/j.scitotenv.2020.143458>.
- Zhang, X., Liu, Y., Zheng, L., Zhang, Q., Li, C., 2021. Simultaneous degradation of high concentration of citric acid coupled with electricity generation in dual-chamber microbial fuel cell. *Biochem. Eng. J.* 173, 108095. <https://doi.org/10.1016/j.bej.2021.108095>.
- Zhe, Y., Cheng, H., Ding, D., He, Y., Ma, Z., Shen, J., 2025. Selective Evolution of Methanogenic Communities by  $\beta$ -lactam Antibiotics Promotes Methane Production. <https://doi.org/10.1128/spectrum.01693-24>.
- Zhen, G., Lu, X., Li, Y.Y., Liu, Y., Zhao, Y., 2015. Influence of zero valent scrap iron (ZVSI) supply on methane production from waste activated sludge. *Chem. Eng. J.* 263, 461–470. <https://doi.org/10.1016/j.cej.2014.11.003>.
- Zhu, D., Wang, Z., Liu, K., Si, B., Yang, G., Tian, C., Zhang, Y., 2023. Multi-cycle anaerobic digestion of hydrothermal liquefaction aqueous phase: role of carbon and iron based conductive materials in inhibitory compounds degradation, microbial structure shaping, and interspecies electron transfer regulation. *Chem. Eng. J.* 454, 140019. <https://doi.org/10.1016/j.cej.2022.140019>.
- Zhu, X., Chen, L., Chen, Y., Cao, Q., Liu, X., Li, D., 2020. Effect of H<sub>2</sub> addition on the microbial community structure of a mesophilic anaerobic digestion system. *Energy* 198, 117368. <https://doi.org/10.1016/j.energy.2020.117368>.